

- L. M. Obeid, *J. Biol. Chem.* **270**, 30701 (1995).
10. K. A. Dressler, S. Mathias, R. N. Kolesnick, *Science* **255**, 1715 (1992); A. Haimovitz-Friedman *et al.*, *J. Exp. Med.* **180**, 525 (1994); M. G. Cifone *et al.*, *ibid.*, p. 1547; S. Mathias *et al.*, *Science* **259**, 519 (1993).
 11. M.-Y. Kim, C. Linardic, L. Obeid, Y. Hannun, *J. Biol. Chem.* **266**, 484 (1991); N. Andrieu, R. Salvayre, T. Levade, *Biochem. J.* **303**, 341 (1994); C. G. Tepper *et al.*, *Proc. Natl. Acad. Sci. U.S.A.* **92**, 8443 (1995).
 12. E. R. Smith and A. H. Merrill Jr., *J. Biol. Chem.* **270**, 18749 (1995).
 13. L. R. Ballou, C. P. Chao, M. A. Holness, S. C. Barker, R. Raghov, *ibid.* **267**, 20044 (1992); J. Q. Chen, M. Nikolova-Karakashian, A. H. Merrill Jr., E. T. Morgan, *ibid.* **270**, 25233 (1995); F. Yanaga and S. P. Watson, *Biochem. J.* **298**, 733 (1994); T. Okazaki, R. M. Bell, Y. A. Hannun, *J. Biol. Chem.* **264**, 19076 (1989); T. Okazaki, A. Bielawska, R. M. Bell, Y. A. Hannun, *ibid.* **265**, 15823 (1990); R. T. Dobrowsky, M. H. Werner, A. M. Castellino, M. V. Chao, Y. A. Hannun, *Science* **265**, 1596 (1994); R. T. Dobrowsky, G. M. Jenkins, Y. A. Hannun, *J. Biol. Chem.* **270**, 22135 (1995).
 14. S. Jayadev *et al.*, *J. Biol. Chem.* **270**, 2047 (1995); G. S. Dbaibo *et al.*, unpublished observations.
 15. C. M. Linardic and Y. A. Hannun, *J. Biol. Chem.* **269**, 23530 (1994); N. Andrieu, R. Salvayre, T. Levade, *Eur. J. Biochem.* **236**, 738 (1996).
 16. P. S. Liu and R. G. W. Anderson, *J. Biol. Chem.* **270**, 27179 (1995).
 17. A. Bielawska, C. M. Linardic, Y. A. Hannun, *FEBS Lett.* **307**, 211 (1992); L. M. Obeid, C. M. Linardic, L. A. Karolak, Y. A. Hannun, *Science* **259**, 1769 (1993); W. D. Jarvis *et al.*, *Proc. Natl. Acad. Sci. U.S.A.* **91**, 73 (1994).
 18. A. Bielawska, H. M. Crane, D. Liotta, L. M. Obeid, Y. A. Hannun, *J. Biol. Chem.* **268**, 26226 (1993).
 19. L. Riboni, R. Bassi, S. Sonnino, G. Tettamanti, *FEBS Lett.* **300**, 188 (1992); A. H. Merrill Jr. *et al.*, *J. Biol. Chem.* **261**, 12610 (1986); A. H. Merrill Jr. and E. Wang, *Methods Enzymol.* **209**, 427 (1992); W. D. Jarvis, A. J. Turner, L. F. Povirk, R. S. Traylor, S. Grant, *Cancer Res.* **54**, 1707 (1994); C. S. S. Rani *et al.*, *J. Biol. Chem.* **270**, 2859 (1995); A. Bielawska *et al.*, *ibid.* **271**, 12646 (1996).
 20. A. Gómez-Muñoz, D. W. Waggoner, L. O'Brien, D. N. Brindley, *J. Biol. Chem.* **270**, 26318 (1995); G. Dbaibo *et al.*, *Proc. Natl. Acad. Sci. U.S.A.* **92**, 1347 (1995).
 21. R. A. Wolff, R. T. Dobrowsky, A. Bielawska, L. M. Obeid, Y. A. Hannun, *J. Biol. Chem.* **269**, 19605 (1994).
 22. A. Gómez-Muñoz, A. Martin, L. O'Brien, D. N. Brindley, *ibid.*, p. 8937; T. Nakamura *et al.*, *ibid.*, p. 18384; M. E. Venable, G. C. Blobe, L. M. Obeid, *ibid.*, p. 26040; Z. Kiss and E. Deli, *FEBS Lett.* **365**, 146 (1995); M. J. Jones and A. W. Murray, *J. Biol. Chem.* **270**, 5007 (1995); Y. Nakamura *et al.*, *J. Immunol.* **156**, 256 (1996); K. Wong, X.-B. Li, N. Hunchuk, *J. Biol. Chem.* **270**, 3056 (1995).
 23. J. Quintans, J. Kilkus, C. L. McShan, A. R. Gottschalk, G. Dawson, *Biochem. Biophys. Res. Commun.* **202**, 710 (1994); M. Chen *et al.*, *Cancer Res.* **55**, 991 (1995); S. J. Martin *et al.*, *EMBO J.* **14**, 5191 (1995); H. Sawai *et al.*, *J. Biol. Chem.* **270**, 27326 (1995); B. Brugg, P. P. Michel, Y. Agid, M. Ruberg, *J. Neurochem.* **66**, 733 (1996).
 24. M. J. Smyth *et al.*, *Biochem. J.* **316**, 25 (1996); S. J. Martin *et al.*, *J. Biol. Chem.* **270**, 6425 (1995).
 25. J. Zhang *et al.*, *Proc. Natl. Acad. Sci. U.S.A.* **93**, 5325 (1996).
 26. S. J. Martin *et al.*, *Cell Death Differ.* **2**, 253 (1995).
 27. A. Ito and K. Horigome, *J. Neurochem.* **65**, 463 (1995); Y. Goodman and M. P. Mattson, *ibid.* **66**, 869 (1996).
 28. M. A. Raines, R. N. Kolesnick, D. W. Golde, *J. Biol. Chem.* **268**, 14572 (1993).
 29. J. K. Westwick, A. E. Bielawska, G. Dbaibo, Y. A. Hannun, D. A. Brenner, *ibid.* **270**, 22689 (1995); S. Pyne, J. Chapman, L. Steele, N. J. Pyne, *Eur. J. Biochem.* **237**, 819 (1996); K. M. Latinis and G. A. Korotetzky, *Blood* **87**, 871 (1996).
 30. M. Verheij *et al.*, *Nature* **380**, 75 (1996).
 31. S. Schütze, T. Machleidt, M. Krönke, *J. Leukocyte Biol.* **56**, 533 (1994); S. Schütze *et al.*, *Cell* **71**, 765 (1992).
 32. G. Dbaibo, L. M. Obeid, Y. A. Hannun, *J. Biol. Chem.* **268**, 17762 (1993); J. C. Betts, A. B. Agranoff, G. J. Nabel, J. A. Shayman, *ibid.* **269**, 8455 (1994).
 33. Z. Yang, M. Costanzo, D. W. Golde, R. N. Kolesnick, *ibid.* **268**, 20520 (1993); S. A. G. Reddy *et al.*, *ibid.* **269**, 25369 (1994).
 34. J.-P. Jaffrézou *et al.*, *Biochim. Biophys. Acta Mol. Cell Res.* **1266**, 1 (1995); M. Higuchi, S. Singh, J.-P. Jaffrézou, B. B. Aggarwal, *J. Immunol.* **157**, 297 (1996).
 35. K. Kuno, K. Sukegawa, Y. Ishikawa, T. Orii, K. Matsushima, *Int. Immunol.* **6**, 1269 (1994).
 36. R. E. Pagano, M. A. Sepanski, O. C. Martin, *J. Cell Biol.* **109**, 2067 (1989); A. G. Rosenwald and R. E. Pagano, *J. Biol. Chem.* **268**, 4577 (1993); F. J. Field, H. Chen, E. Born, B. Dixon, S. Mathur, *J. Clin. Invest.* **92**, 2609 (1993); C. M. Linardic, S. Jayadev, Y. A. Hannun, *J. Biol. Chem.* **267**, 14909 (1992); T. Oda, C.-H. Chen, H. C. Wu, *ibid.* **270**, 4088 (1995); C. M. Linardic, S. Jayadev, Y. A. Hannun, *Cell Growth Differ.* **7**, 765 (1996).
 37. L. Riboni, A. Prinetti, R. Bassi, A. Caminiti, G. Tettamanti, *J. Biol. Chem.* **270**, 26868 (1995).
 38. M. Hayakawa, S. Jayadev, M. Tsujimoto, Y. A. Hannun, F. Ito, *Biochem. Biophys. Res. Commun.* **220**, 681 (1996); Y. Chang, A. Abe, J. A. Shayman, *Proc. Natl. Acad. Sci. U.S.A.* **92**, 12275 (1995).
 39. N. D. Ridgway, *Biochim. Biophys. Acta Lipids Lipid Metab.* **1256**, 39 (1995); P. Santana *et al.*, *Endocrinology* **136**, 2345 (1995).
 40. J. C. Strum, K. I. Swenson, J. E. Turner, R. M. Bell, *J. Biol. Chem.* **270**, 13541 (1995).
 41. S. J. F. Lauderkind, A. Bielawska, R. Raghov, Y. A. Hannun, L. R. Ballou, *J. Exp. Med.* **182**, 599 (1995).
 42. R. T. Dobrowsky and Y. A. Hannun, *J. Biol. Chem.* **267**, 5048 (1992); R. T. Dobrowsky, C. Kamibayashi, M. C. Mumby, Y. A. Hannun, *ibid.* **268**, 15523 (1993); B. Law and S. Rossie, *ibid.* **270**, 12808 (1995); R. T. Dobrowsky and Y. A. Hannun, *Adv. Lipid Res.* **25**, 91 (1993).
 43. J. T. Nickels and J. R. Broach, *Genes Dev.* **10**, 382 (1996).
 44. J. D. Fishbein, R. T. Dobrowsky, A. Bielawska, S. Garrett, Y. A. Hannun, *J. Biol. Chem.* **268**, 9255 (1993).
 45. G. Müller *et al.*, *EMBO J.* **14**, 1961 (1995); J. Lozano *et al.*, *J. Biol. Chem.* **269**, 19200 (1994).
 46. C. K. Joseph, H.-S. Byun, R. Bittman, R. N. Kolesnick, *J. Biol. Chem.* **268**, 20002 (1993); S. Mathias, K. A. Dressler, R. N. Kolesnick, *Proc. Natl. Acad. Sci. U.S.A.* **88**, 10009 (1991).
 47. M. Faucher, N. Girones, Y. A. Hannun, R. M. Bell, R. Davis, *J. Biol. Chem.* **263**, 5319 (1988); T. Goldkorn *et al.*, *ibid.* **266**, 16092 (1991).
 48. J. Liu, S. Mathias, Z. Yang, R. N. Kolesnick, *ibid.* **269**, 3047 (1994).
 49. T. Okazaki, A. Bielawska, N. Domae, R. M. Bell, Y. A. Hannun, *ibid.*, p. 4070; M. W. Spence, *Adv. Lipid Res.* **26**, 3 (1993); S. Chatterjee, *ibid.*, p. 25.
 50. S. Jayadev, C. M. Linardic, Y. A. Hannun, *J. Biol. Chem.* **269**, 5757 (1994).
 51. J. W. Larrick and S. C. Wright, *FASEB J.* **4**, 3215 (1990); M. Hayakawa *et al.*, *J. Biol. Chem.* **268**, 11290 (1993).
 52. G. J. Pronk, K. Ramer, P. Amiri, L. T. Williams, *Science* **271**, 808 (1996).
 53. A. Kalén, R. A. Borchardt, R. M. Bell, *Biochim. Biophys. Acta Lipids Lipid Metab.* **1125**, 90 (1992); R. Bose *et al.*, *Cell* **82**, 405 (1995).
 54. J.-P. Jaffrézou *et al.*, *EMBO J.* **15**, 2417 (1996).
 55. G. Dbaibo, M. Pushkareva, N. Alter, M. Smyth, L. Obeid, Y. Hannun, unpublished observations.
 56. Supported by NIH (grant GM43825), the U.S. Department of Defense (DAMD17-94J4301), and the American Cancer Society (CB122). I thank L. Obeid for a careful and critical review of the manuscript.

RESEARCH ARTICLE

Structure of Staphylococcal α -Hemolysin, a Heptameric Transmembrane Pore

Langzhou Song,* Michael R. Hobaugh,* Christopher Shustak, Stephen Cheley, Hagan Bayley, J. Eric Gouaux†

The structure of the *Staphylococcus aureus* α -hemolysin pore has been determined to 1.9 Å resolution. Contained within the mushroom-shaped homo-oligomeric heptamer is a solvent-filled channel, 100 Å in length, that runs along the sevenfold axis and ranges from 14 Å to 46 Å in diameter. The lytic, transmembrane domain comprises the lower half of a 14-strand antiparallel β barrel, to which each protomer contributes two β strands, each 65 Å long. The interior of the β barrel is primarily hydrophilic, and the exterior has a hydrophobic belt 28 Å wide. The structure proves the heptameric subunit stoichiometry of the α -hemolysin oligomer, shows that a glycine-rich and solvent-exposed region of a water-soluble protein can self-assemble to form a transmembrane pore of defined structure, and provides insight into the principles of membrane interaction and transport activity of β barrel pore-forming toxins.

The α -hemolysin (α HL) of the human pathogen *Staphylococcus aureus* is secreted as a 33.2-kD water-soluble monomer that binds to rabbit erythrocytes and human platelets, erythrocytes, monocytes, lympho-

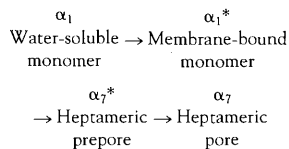
cytes, and endothelial cells (1). Membrane-bound monomers assemble to form 232.4-kD heptameric transmembrane pores (2). The sensitivity of cells to α HL ranges from human erythrocytes, which require solution

concentrations of α HL above 1 μ M for lysis, to human platelets and rabbit erythrocytes, which are lysed at 1 nM (3). The heptamer is the cytolytic species, and primary mechanisms of cell death include (i) bilayer permeabilization to ions, water, and low molecular weight molecules, and (ii) cell lysis (1).

The conductance of α HL pores displays a near linear dependence on solution conductivity and is thus suggestive of a water-filled channel (4). An effective diameter of 11.4 ± 0.4 Å has been estimated from the conductance of single oligomers (about 90 pS, +15 mV, 0.1 M KCl, pH 7.0) (4). Assembled on cell membranes α HL channels exhibit partial rectification, modest anion selectivity and rapid fluctuations to a higher single channel conductance state at acidic pH (4–6). Spectral analysis of pH-dependent fluctuations in current are consistent with a model in which about four identical ionizable groups ($pK_a \approx 5.5$) reside in the channel (6). In addition, low pH and di- and trivalent cations cause slow, reversible voltage-dependent channel closure (4, 5).

α HL assembles on cellular and synthetic membranes (7, 8), whereas deoxycholate (9) or diheptanoylphosphatidyl choline (DiC₇PC) micelles (10) catalyze heptamer formation in solution. Even though the monomer is highly soluble in aqueous solution (~0.3 mM) and the primary structure is polar with no obvious hydrophobic transmembrane stretches (11), the heptamer is amphiphilic and firmly rooted to the membrane. The heptamer is not released into aqueous solution by high salt, basic pH, or chaotropic agents, and solubilization of the membrane-bound heptamer requires detergent micelles (9, 12).

A host of experimental approaches has illuminated a mechanistic framework for the assembly of α HL (see below) and has pinpointed residues involved in membrane binding, assembly, and in defining the transmembrane pore.



Circular dichroism shows that the primarily β secondary structure does not undergo large changes during the conversion of α_1 to

α_7 (13). Nonetheless, the amino latch (Ala¹-Val²⁰) and the glycine-rich region (Lys¹¹⁰-Tyr¹⁴⁸), which are susceptible to trypsin and proteinase K in α_1 , are protease resistant after α_7 formation (14). The α_1^* and α_7^* intermediates remain sensitive to proteolysis at the amino latch, and the glycine-rich region is not attacked (15). Hallmarks of the α_7^* prepore are that it is nonlytic, does not form transmembrane pores, and is heptameric in subunit stoichiometry (15). Recent studies suggest that the glycine-rich region inserts into the bilayer (16) and lines the transmembrane channel (17) and that His³⁵ is a critical residue (18–22) that becomes buried after α_7 formation (19). In the α_7^* to α_7 step, a functional pore is formed, the glycine-rich region is translocated across the membrane (23), and the amino latch becomes protease resistant (15). Thus membrane translocation and pore formation follow oligomerization.

In function, α HL is related to bacterial toxins that include aerolysins from *Aeromonas hydrophila* and *A. sobria*, and α toxin from *Clostridium septicum*. These toxins assemble from water-soluble species to form transmembrane pores that disrupt the membranes of their hosts, cause leakage of low

molecular weight molecules, destroy cellular osmotic balance, and promote cell lysis (24). Eukaryotic proteins such as perforin and complement C9, although distinct in terms of sequence and size, also assemble to oligomeric transmembrane pores (25).

We now present a high-resolution, three-dimensional structure of an assembled pore-forming toxin. In particular, we describe the molecular structure of the detergent-solubilized α HL heptamer at 1.9 Å resolution. This high-resolution structure defines the architecture of the pore-forming motif and its surrounding scaffold, and it provides a structural basis for understanding protein-bilayer interactions, heptamer assembly, membrane insertion and the biophysical properties of the channel.

Structure determination and molecular architecture. A crystallization strategy designed for membrane proteins that included full factorial and sparse sampling matrices yielded 22 distinct crystal forms with the heptamer (26) solubilized in five detergents (2, 27). Of these crystal forms, five diffract to at least 3 Å resolution, and one form, grown in the presence of *n*-octyl- β -glucoside, ammonium sulfate, and PEG 5000 monomethyl ether and diffracting to 1.8 Å

Table 1. Statistics for data collection, phase determination and refinement. The crystals are in space group C2, with unit cell dimensions of $a = 151.92$ Å; $b = 136.76$ Å; $c = 135.12$ Å; $\beta = 91.38^\circ$.

Item	Native II	Native I	UO ₂ Cl ₂	OsCl ₃	K ₂ OsO ₄	K ₃ IrCl ₆
Detector, $\lambda = 1.54$ Å	R-Axis IIC	FAST				
d min (Å)	1.89	2.39	3.0	3.5	3.5	4.0
Unique reflections (N)	206863	94796	41345	30594	33480	22452
Observations (N)	2924665	389970	55339	79989	111484	83467
Mean redundancy	14.1	4.1	1.4	2.6	3.3	3.7
Data coverage (%)	93.3	89.5	52.8	87.7	95.9	96.5
R_{sym} (I) (%) [*]	8.4	6.2	8.1	4.1	6.0	4.2
Mean fractional isomorphous difference (%) [†]			27.1	13.0	14.0	25.1
MIR analysis						
d min (Å)			3.0	3.5	3.5	4.0
Heavy atom sites (unit cell) (N)			80	80	36	60
Phasing power [‡]			1.61	2.14	1.72	1.46
R_{cullis} [§]			0.67	0.69	0.67	0.77
Mean overall figure of merit		0.504				
Refinement (Native II)						
Model: 2051 residues, 818 water molecules (17214 atoms)						
					rms deviations	
d -spacings (Å)	Reflections (N)	R value [¶] (%)	Free R -value (%)	Bonds (Å)	Angles (°)	B values (Å ²)
8.0–1.9	198341	19.9	25.7	0.012	1.66	2.23

L. Song, M. R. Hobaugh, and J. E. Gouaux are in the Department of Biochemistry and Molecular Biology, The University of Chicago, 920 East 58 Street, Chicago, IL 60637, USA. C. Shustak, S. Cheley, and H. Bayley are with the Worcester Foundation for Biomedical Research, 222 Maple Avenue, Shrewsbury MA 01545, USA.

*These authors made equal contributions to this work. †Present address: Department of Biochemistry and Molecular Biophysics, Columbia University, 650 West 168 Street, New York, NY 10032, USA.

^{*} $R_{\text{sym}} = \frac{1}{N} \sum_{hkl} \sum_i |I(hkl) - \overline{I(hkl)}| / I(hkl)$. †Mean fractional isomorphous difference = $\frac{1}{N} \sum_{hkl} \sum_i (|F_{PH}| - |F_P|) / |F_P|$. $|F_P|$ is the protein structure factor amplitude and $|F_{PH}|$ is the heavy-atom derivative structure factor amplitude. ‡Phasing power = $\text{rms} (|F_H|/E)$, where $|F_H|$ = heavy-atom structure factor amplitude and E = residual lack of closure error. § $R_{\text{cullis}} = \frac{1}{N} \sum_{hkl} \sum_i (|F_{PH} \pm F_P| - F_{H(\text{calc})}) / |F_{PH} \pm F_P|$ where F_H is the calculated heavy atom structure factor contribution. ||Mean overall figure of merit = $|F(hkl)_{\text{best}}| / I(hkl)$. ¶ R values: Crystallographic R value ($\frac{1}{N} \sum_{hkl} \sum_i |F_o| - |F_c| / \sum_i |F_o|$) with 90 percent of the native data employed for refinement. Free R value: R value based on 10 percent of the native data withheld from refinement. *Rms bond lengths and bond angles are the rms deviations from ideal values for bond lengths and angles, respectively. †Rms deviations on B-values are the rms mean-square deviation between B-values on covalently bonded atom pairs.

resolution, was used to solve the structure.

The initial phases were obtained by the multiple isomorphous replacement (MIR) method (28–33). Solvent flattening (34) and histogram matching (35) yielded modest improvements to the initial 3 Å electron density map. Real space averaging around the molecular, seven-fold axis resulted in a dramatic improvement in the MIR-phased electron density map at 3 Å resolution (36). The phases were extended from 3 Å to 1.9 Å resolution in 300 cycles of density modification, which included averaging, solvent flattening, and histogram matching by the program DM (37). The structure (38, 39) has been refined with X-PLOR (40, 41) to a conventional *R* value of 0.199 and a free

R value of 0.257 (Fig. 1 and Table 1). During refinement, the coordinates were not restrained to the noncrystallographic sevenfold axis with the exception of two sections encompassing residues 119 to 140 and 260 to 265 (41). In each protomer there is one cis peptide bond at Pro¹⁰³. The structure includes main chain atoms for all 2051 residues, side chain atoms for all but six residues for which there is no significant electron density, and 818 solvent molecules, which were modeled as waters (42).

The heptameric complex is mushroom-shaped and measures 100 Å in height and up to 100 Å in diameter (Fig. 2). A solvent-filled channel running along the sevenfold axis forms the transmembrane pore.

This aqueous channel spans the length of the complex and ranges from 14 Å to 46 Å in diameter. The gross size and shape of the heptamer resemble low resolution images of αHL assembled on bilayers, although data from electron microscopy and a range of biochemical and biophysical experiments have been incorrectly interpreted in terms of a hexameric subunit stoichiometry (2).

Comprising the heptameric complex are the cap domain, the stem domain and seven rim domains. Electron microscopy of αHL assembled on membranes show large protrusions from the bilayer surface (43), which we identify as the cap domain and portions of the rim domains. The cap domain is composed of seven β sandwiches and the amino latches of each protomer. Rim domains protrude from the underside of the heptamer, participate in only a few protomer-protomer interactions, and are probably in close proximity, if not in direct contact, with the membrane bilayer. The stem domain forms the transmembrane channel. A crevice between the top of the stem domain and the rim domains defines a basic and aromatic amino acid-rich region that might participate in interactions with phospholipid head groups or other cell surface receptors. Extensive hydrophobic and hydrophilic contacts throughout the cap knit the protomers together and form interdigitating networks that confer stability on the heptamer.

The primary structure, corresponding elements of secondary structure, and diagrams of a protomer are shown in Fig. 3. The protomers adopt a tertiary fold that is dis-

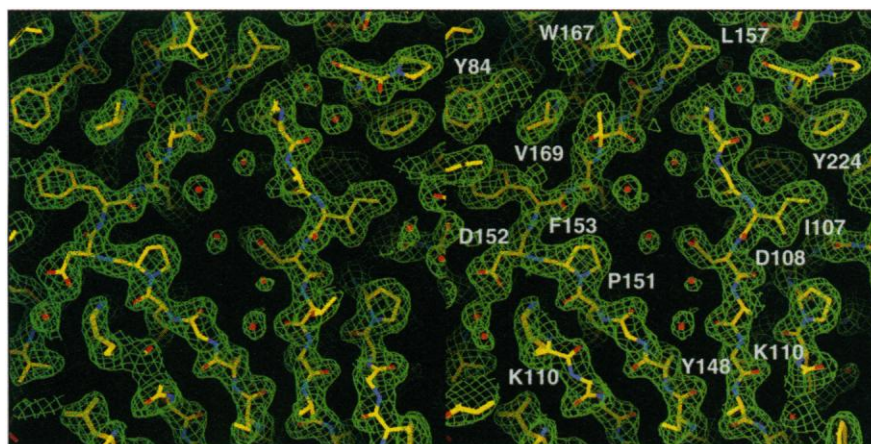
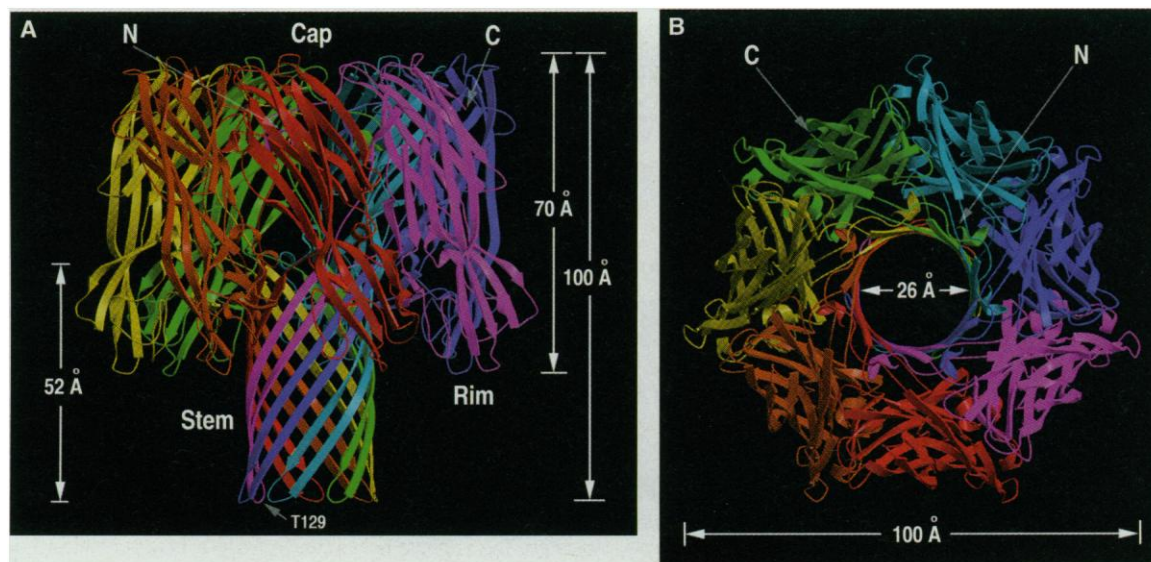


Fig. 1. Stereo diagram of the electron density distribution in the triangle region calculated with $2|F_o| - |F_c|$ coefficients and phases from the refined model contoured at 1σ . The separation of the polypeptide chain from a protomer core to form the stem β strands (bottom of view) is evident in the electron density. Solvent molecules modeled as waters are indicated by red spheres.

Fig. 2. Ribbon representations of the αHL heptamer with each protomer in a different color. (A) View perpendicular to the sevenfold axis and approximately parallel to the putative membrane plane. The mushroom-shaped complex is approximately 100 Å tall and up to 100 Å in diameter, and the stem domain measures about 52 Å in height and 26 Å in diameter from C_α to C_α. Approximate locations of the cap, rim, and stem domains are shown. Thr¹²⁹ is located at the base of the stem domain.



(B) View from the top of the structure and parallel to the sevenfold axis. The amino latch of one protomer makes extensive interactions with its clockwise-related immediate neighbor and residues in each glycine-rich region wrap around the sevenfold axis approximately 180°. Protomer-

protomer contacts consist almost exclusively of side chain-side chain interactions in the cap domain while in the stem domain main chain-main chain contacts predominate as the β strands form a continuous β sheet.

tinct from folds previously described (44). Contained within the protomer core are the elements of structure that constitute the β sandwich and rim domains. Approximately 80 percent of the amino acids form the protomer core, which is an ellipsoid that measures 70 Å along the sevenfold axis, 45 Å wide and 20 Å thick. Superpositions of protomers in crystallographically independent environments indicate that they have the same fold and very similar conformations; the mean root mean square (rms) deviation between protomer A and the other six protomers is 0.24 Å for main chain

atoms. Each protomer is composed of 16 β strands (52.9 percent), four short stretches of either α - or 3_{10} -helix (4.3 percent), a long region of random coil that spans residues Asp¹⁸³ through Lys²⁰⁵ (7.9 percent) and substantial non- α , non- β elements of structure (34.9 percent), in agreement with estimates from circular dichroism studies (13, 45). Pronounced excursions of the polypeptide chain from the protomer core include the amino latch (Ala¹-Val²⁰), and 39 residues (Lys¹¹⁰ to Tyr¹⁴⁸), which form the stem domain. Linking the stem β strands to the protomer core are two short

sections of polypeptide that form two sides of the triangle region (Pro¹⁰³ to Thr¹⁰⁹ and Val¹⁴⁹ to Asp¹⁵²), an element of structure which participates in crucial protomer-protomer interactions and may play a key role in conformational rearrangements that accompany the conversion of α_1 to α_7 .

The transmembrane stem is composed of 14 antiparallel β strands, two of which are contributed by each protomer (Fig. 4). These strands begin at Lys¹¹⁰ and end at Tyr¹⁴⁸, and they form a righthand barrel with a height of 52 Å and a diameter of 26 Å, measured from α -carbon positions. Each

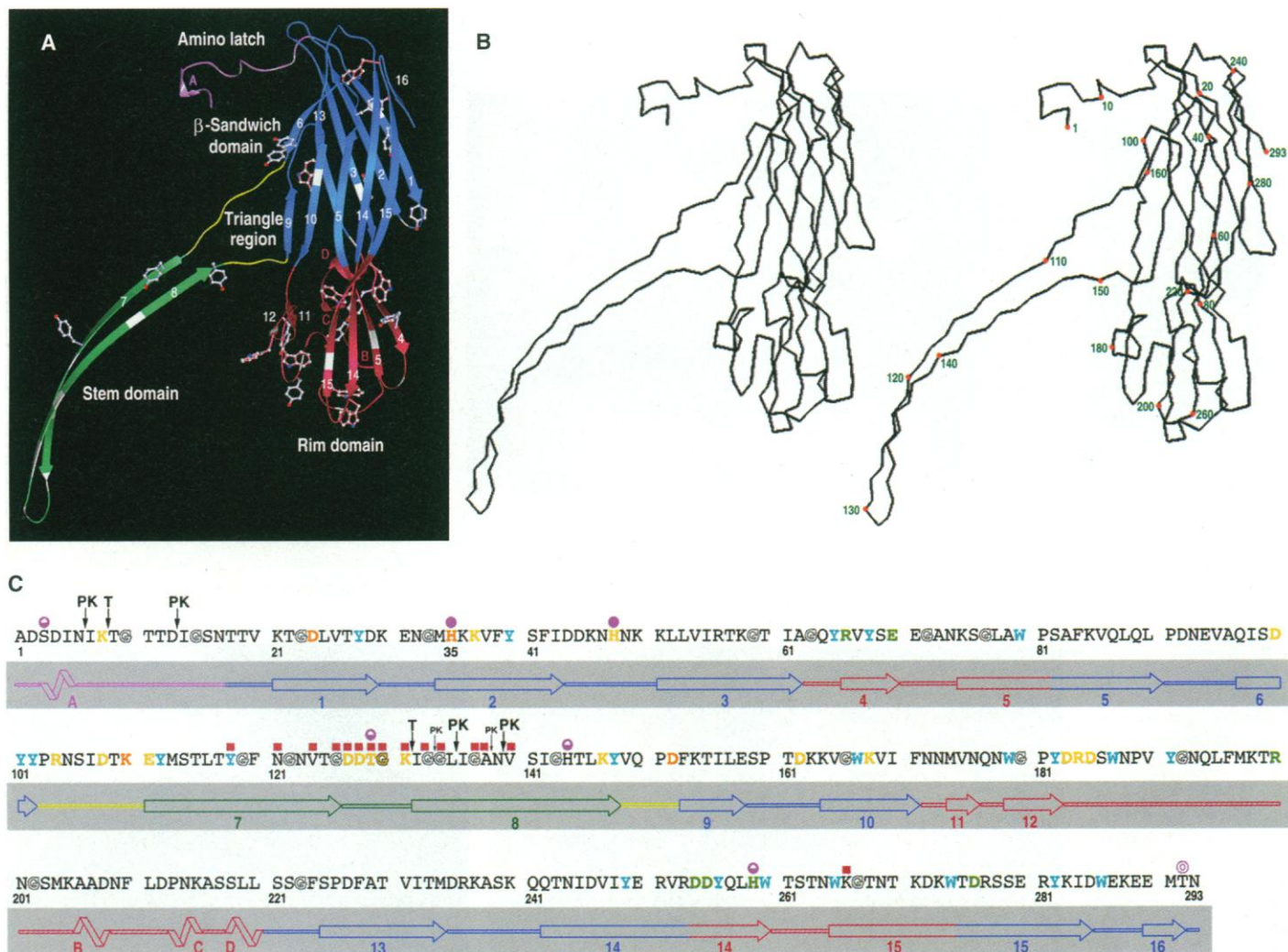


Fig. 3. (A) Ribbon diagram of an isolated protomer with β strands numbered consecutively. This view is from the “outside” of the heptamer. The β -sandwich domain (blue) is a scaffold for the protomer core and is formed by two antiparallel β sheets that we define as the inner (strands 1, 2, 3, 13, 6) and outer (strands 9, 10, 5, 14, 15, 16) sheets, located on the interior and exterior of the cap domain, respectively. The rim domain (red), Tyr and Trp residues and glycines (white swatches on the ribbon and rope) are also indicated. The β strands that compose the stem domain are green. **(B)** Stereoview of a protomer oriented similarly to the schematic in (A). **(C)** Correspondence between the primary sequence and protomer secondary structure with emphasis of important residues. Red squares define acrylodan-derivatized single cysteine mutants in which the label is in a more hydrophobic environ-

ment following heptamer formation on membranes (52). Single cysteine mutations at the orange sites have a major effect on activity without chemical modification and at the yellow sites represent positions where effects are seen only after chemical modification (20). Residues colored green are involved in cell binding based on mutagenesis and chemical modification studies (20, 22). Purple circles indicate sites whose reactivity changes on heptamer formation in site-directed chemical modification experiments; (half-filled circles) highly reactive to less reactive; (filled circles) highly reactive to unreactive; (outlined circles) low reactivity to higher reactivity. Abbreviations for the amino acid residues are: A, Ala; C, Cys; D, Asp; E, Glu; F, Phe; G, Gly; H, His; I, Ile; K, Lys; L, Leu; M, Met; N, Asn; P, Pro; Q, Gln; R, Arg; S, Ser; T, Thr; V, Val; W, Trp; and Y, Tyr.

strand wraps around the barrel axis by approximately 180° . In contrast to the $n = 16$ and $n = 18$ β barrels found in the bacterial porins (46, 47), which have shear numbers (S) (48) of 20 and 22 ($S = n + 4$), respectively, the α HL stem β barrel has a shear number of 14 ($S = n$). For α HL, the β strands are not tilted as far from the barrel axis ($\alpha \approx 38^\circ$) as are the β strands in barrels with shear numbers of $S = n + 4$ ($\alpha \approx 45^\circ$). Large β barrels ($n > 8$) with $S = n$ have apparently not been observed before our

structure determination (48). However, we propose that homomeric β barrels where each protomer contributes two strands are likely to have shear numbers of $S = n$. The electron density for residues 119 to 140 is relatively weak, and this glycine-rich region is characterized by high thermal parameters (about 70 \AA^2). Nonetheless, sevenfold averaged electron density maps enabled us to obtain a reliable trace through this region and allowed for the placement of amino acid side chains.

Pore, interprotomer and membrane surfaces. At the top of the cap domain, the $\sim 28 \text{ \AA}$ channel diameter is lined by the amino latches (Fig. 4). Within the cap domain, the inner sheets of the β -sandwich domains form the walls of the widening pore. At the vertex of the triangle marked by Pro¹⁰³, the channel reaches a maximum diameter of 46 \AA . The channel narrows to $\sim 15 \text{ \AA}$ in diameter at the juncture of the triangle and the stem. Through the stem, the diameter of the channel varies from 14 to 24 \AA , depending on the volume of the side chains protruding into the 26 \AA (C_α - C_α) diameter cylinder. Both ends of the stem are defined by rings of acidic and basic residues, and the intervening 40 \AA is lined by neutral amino acids. Two hydrophobic bands, one formed by seven Met¹¹³ residues and the second by seven Leu¹³⁵ residues, are solvent-exposed on the interior of the pore and demonstrate that hydrophobic residues contribute to the lining of transmembrane channels. The distribution of rings of negatively and positively charged residues, in combination with the bands of hydrophobic groups, are reminiscent of the proposed arrangement of polar and nonpolar groups in the channel of the nicotinic acetylcholine receptor (49).

Each promoter is involved in about 120 salt bridges and hydrogen bonds, participates in about 850 van der Waals contacts, and buries almost one-third of the solvent accessible surface area in the heptamer (Table 2). Both polar and nonpolar interactions are present in the five major interfaces although the stem domain has a preponderance of main chain hydrogen bonds. Most (>98 percent) of the contacts occur be-

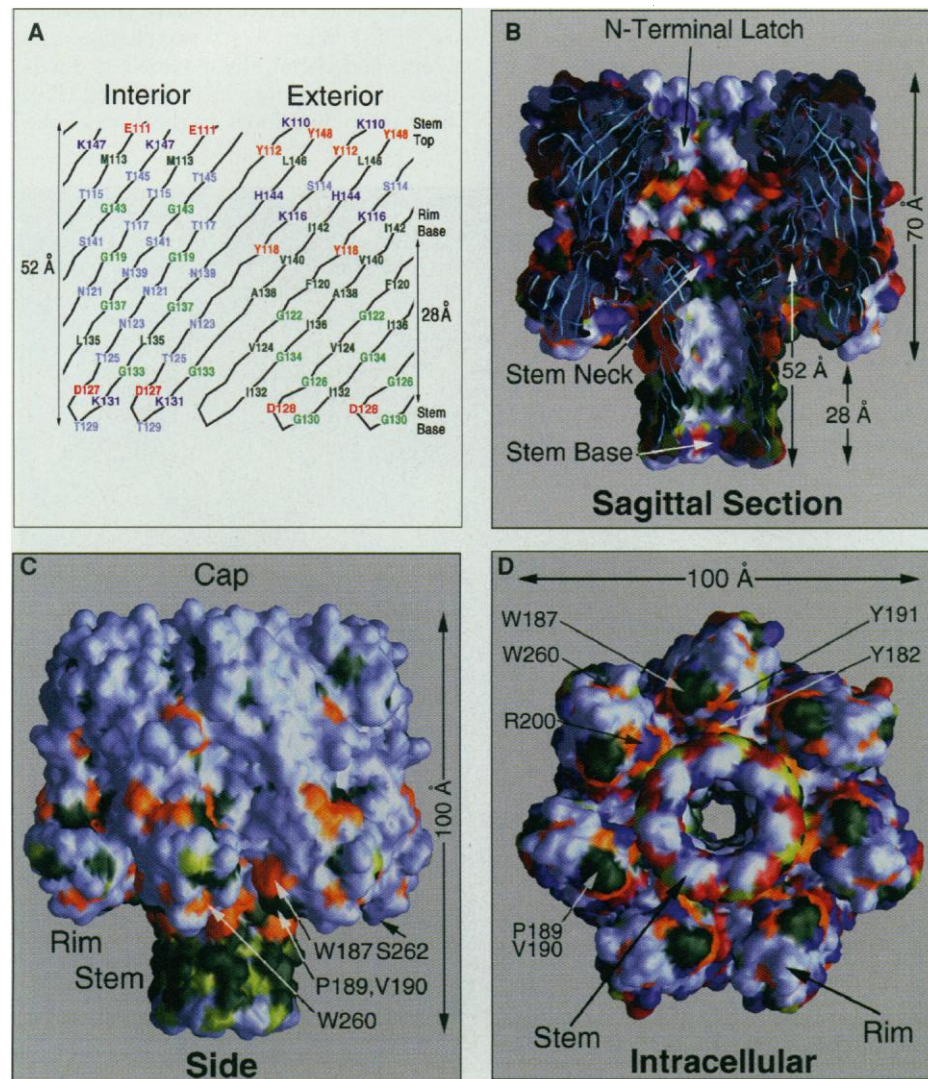


Fig. 4. (A) Schematic representation of the residues that define the inner and outer surfaces of the stem domain. The α -carbons of the stem were projected onto the surface of a cylinder that was then unrolled. Residues are color coded: Ala, Val, Pro, Leu, Ile, Met, Phe: dark green; Gly: light green; Asp, Glu: red; Lys, Arg, His: blue; Tyr, Trp: gold; Ser, Thr, Asn, Gln: light purple. In the left and right vertical strips are the residues whose α -carbons project β -substituents to the interior and exterior of the channel, respectively. (B) Solvent accessible surfaces of α -C, colored by the same code as Fig. 4A. Sagittal section along the seven-fold axis. The protein residues lining the channel are predominately charged or polar. (C) Side view. The polar and charged character of the cap contrasts with the primarily nonpolar surface of the stem exterior. Aromatic residues and nonpolar amino acids on the rim domain, such as Trp¹⁸⁷, Pro¹⁸⁹, Val¹⁹⁰, and Trp²⁶⁰, may interact with the membrane. The color coding is the same as in (A) except that Asp, Glu, Lys, Arg, His, Ser, Thr, Asn, and Gln are light purple. (D) Intracellular view. This is a view from the membrane looking toward the putative membrane binding surface. The bases of the seven rim domains and the stem-rim crevice have a preponderance of aromatic and basic residues, suggestive of rim-membrane interactions.

Table 2. Buried interprotomer surfaces. Reduction in the solvent accessible surface area on the hypothetical assembly of a heptamer from regions or domains of a protomer. These values were obtained by calculating the surface area of the protomer (area A, 17,120 \AA^2). The domain or region of interest was abstracted from the coordinate file and its solvent-accessible surface was computed (area B). Then the combined area of the protomer and domain or region was calculated (area C). The reduction in solvent-accessible surface area is then defined as $(A + B - C)/2$. Since a protomer forms interactions with both its +1 and -1 neighbors, the total reduced surface area is approximately 5664 \AA^2 . The radius of the probe was 1.4 \AA and the calculations were performed with the use of GRASP.

Domains or regions	Surface area (\AA^2)
Amino latch	670
β sandwich	851
Rim	90
Triangle	410
Stem	811
Total	2832

tween nearest neighbors, and the few (1, 3) interprotomer interactions involve amino latch to β -sandwich and stem top to rim interactions. Key contacts, as determined from our structure and from site-directed mutagenesis, are conserved in each of the seven interfaces and virtually all interprotomer interactions are similar in each crystallographically different interface (Fig. 5).

The amino latch is important for heptamer formation and cell lysis (14). In the heptamer structure, the amino latch makes extensive contacts with the inner β sheet of an adjacent protomer. Deletion of the NH₂-terminal two amino acids abolishes hemolytic activity (14) although individual charged residues in this region do not have essential roles (20). His³⁵ is located in the crucial β -sandwich contact region. Conservative substitutions at position 35 render the protein diminished in lytic, heptamer-forming, and lethal activity, and nonconservative changes abolish these activities (18, 19, 22). Additional groups of interacting residues in this essential interface involve inter β -sandwich contacts between the side chains of His⁴⁸ and Asp²⁴, as well as between Lys³⁷ and Lys⁵⁸ on one protomer with Asp¹⁰⁰ on its neighbor. Asp²⁴, His⁴⁸, and Asp¹⁰⁰ also affect or influence hemolytic activity (20).

The triangle region is the nexus between (i) a protomer core and its stem-forming strands, (ii) triangle regions on adjacent protomers, and (iii) triangle region-rim domains on adjacent protomers. A network of salt bridges and hydrogen bonds link the amino group of Lys¹¹⁰ with the main-chain carbonyl oxygen of Gln¹⁵⁰ and the side-chain residues of Asp¹⁵² and Asn¹⁷³ (rim domain) on an adjacent protomer. Mutagenesis of either Lys¹¹⁰ or Asp¹⁵² to cysteine diminishes or ablates hemolytic activity, respectively (20). Additional interprotomer contacts include polar interactions between Lys¹⁵⁴ and Asn²¹⁴ (rim domain) as well as nonpolar interactions between Ile¹⁰⁷ and Phe¹⁵³ and Leu²¹⁹ (rim domain).

A hydrophobic belt on the stem exterior is defined by residues Tyr¹¹⁸ to Gly¹²⁶ and Ile¹³² to Ile¹⁴² and a ring of 14 aromatic amino acids is composed of Tyr¹¹⁸ and Phe¹²⁰ (Fig. 4). In contrast, the remaining solvent-exposed surfaces of the heptamer are primarily polar and charged. Below the hydrophobic belt is a collar of charged and polar residues (Asp¹²⁷ to Lys¹³¹) that define the base of the stem. Above the hydrophobic belt is a crevice between the stem and rim domains that is highly populated by aromatic residues and positively charged amino acids.

We propose that the hydrophobic belt on the stem domain, which is ~28 Å thick, interacts with the nonpolar portion of the lipid bilayer. The thickness of the hydro-

phobic region of dipalmitoylphosphatidylcholine bilayers is 28 to 30 Å (50) and erythrocyte membranes are rich in phosphatidylcholine and sphingomyelin lipids (16:0, 18:0, 18:1, and 18:2 acyl chains) (51). Thus, the nonpolar belt of the α HL stem is thick enough to span the hydrophobic domain of an erythrocyte bilayer. Reinforcing the assignment of the transmembrane domain are (i) fluorescence studies of α HL site-specifically labeled with acrylodan, a polarity sensitive probe, which suggest that residues Tyr¹¹⁸ to Val¹⁴⁰ comprise the transmembrane sequence (52) and (ii) Förster energy transfer experiments that indicate that position 130 is about 5 Å from the head groups on the inner leaflet (16). In the water-soluble monomer, the residues

comprising the membrane-spanning portion of the stem domain are protease sensitive (13, 14) and solvent exposed (52). Therefore, the α HL heptamer provides a high-resolution, three-dimensional view of how an approximately 20-residue fragment of a water-soluble protein creates a stable transmembrane structure.

Interactions between the heptamer and the lipid head groups involve both the stem and the rim domains (Fig. 6). Difference electron density maps calculated from x-ray diffraction data of α_7 crystals soaked with DiC₇PC showed strong positive peaks near Arg²⁰⁰ (53). When Arg²⁰⁰ was changed to a cysteine and chemically modified, α_1 binding to rabbit erythrocytes is abolished (20). Three protruding loops at the base of the

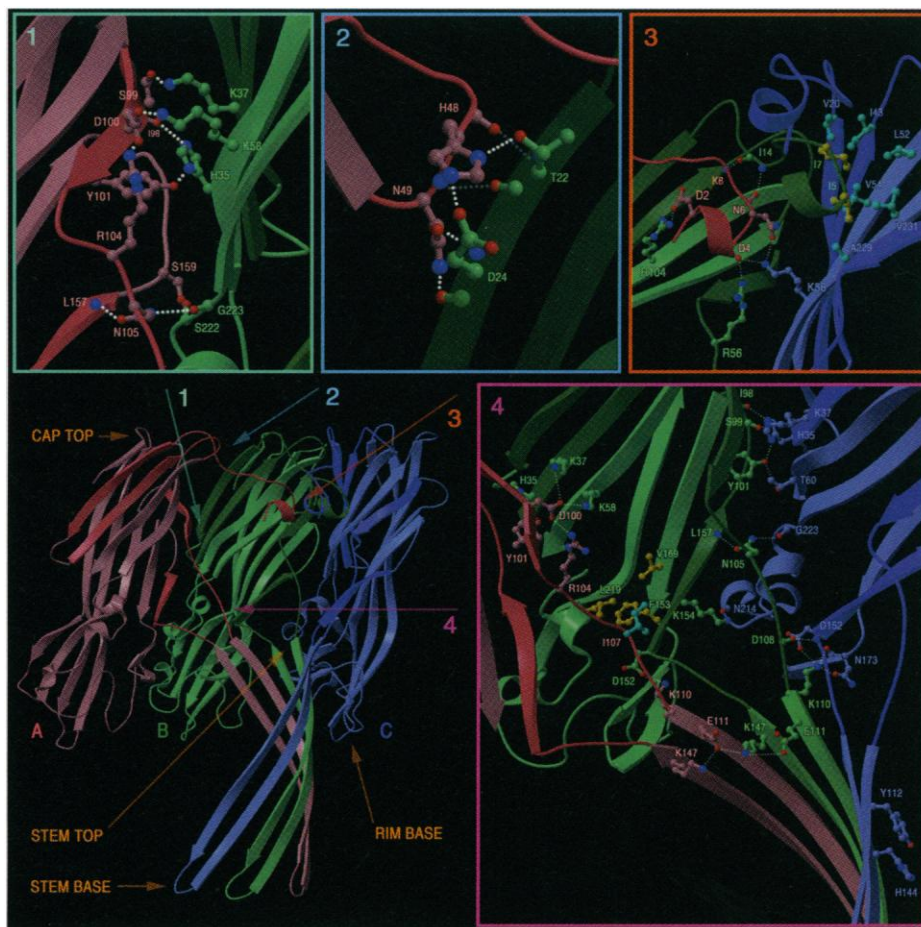


Fig. 5. Schematic dissection of protomer-protomer interactions (A, pink; B, green; C, purple) viewed from the lumen of the pore. Shown in panel 1 are hydrogen bonds and salt links near His³⁵, a residue that defines a region particularly critical for heptamer formation and cell lysis. In 2 are shown the interactions between His⁴⁸ (A) and Asp²⁴ (B) and Thr²² (B). This second region of β -sandwich- β -sandwich contact includes polar interactions between main chain atoms of Asn⁴⁷ O (A) to Thr²² N (B) and Asn⁴⁹ N (A) to Thr²² O (B). As depicted in 3, the amino latches participate in numerous polar and nonpolar contacts. To simplify the view, polar interactions are shown between protomers A (pink) and B (green), and residues involved in nonpolar interactions are defined for protomers B and C (purple). Shown in 4 is a closeup of the interactions in the triangle region of protomer B and their spatial relationship to other important regions. Of particular significance are the polar interactions from Lys¹¹⁰ (B) to Asp¹⁵² (C) and Asn¹⁷³ (C) and from Lys¹⁴⁷ (B) to Glu¹¹¹ (B) and Glu¹¹¹ (A). These interactions involving two consecutive residues at the beginning of the stem domain may help orient the stem β strands. Ile¹⁰⁷ (A) and Phe¹⁵³, Val¹⁶⁹ and Leu²¹⁹ on protomer B form an interprotomer hydrophobic cluster.

rim domains constitute another potential membrane binding site. These loops are composed of neutral and nonpolar residues and are near Trp¹⁸⁷, Pro¹⁹⁰, Val¹⁹¹, Arg²⁰⁰, Met²⁰⁴, and Trp²⁶⁰; and they are flanked by residues that when mutated prevent membrane binding (20). The proximity of the base of the rim domain to the membrane spanning region of the stem, combined with the character of the rim domain surface, leads us to speculate that the base of the rim and the crevice between the rim and stem domains interact with the cell membrane. In fact, fluorescence studies of a single cysteine mutant labeled with acrylodan at position 266 in the rim domain indicate that this site is exposed to a more hydrophobic environment upon heptamer formation (52), thus suggesting membrane insertion.

Molecular basis of transport activity and mechanism of assembly. The α HL heptamer structure provides a basis for understanding the biophysical properties of the pore and forms the basis for detailed mechanistic studies. We find that the narrowest constriction in the pore is ~ 14 Å (Fig. 4), which is in agreement with previous approximations of the pore diameter (4). This constriction is formed by the side chains of Glu¹¹¹, Lys¹⁴⁷, and Met¹¹³, and it probably confers the estimated 2-kD size limit for transport of macromolecules by the pore (54). The ring of Glu¹¹¹ residues, located within the pore and at the top of the stem, forms favorable binding sites for a range of di- and trivalent cations. On incubation of $\alpha 7$ crystals with 5 mM UO₂Cl₂, for example, we observe strong peaks ($> 7\sigma$) in difference Patterson and Fourier maps near the carboxylate groups of Glu¹¹¹. Sim-

ilar features are seen with crystals soaked in solutions containing OsCl₃ and K₃IrCl₆. One mechanism by which di- and trivalent ions effect partial or complete reduction in pore conductance (4, 5) may involve steric block of the channel by ion binding to Glu¹¹¹ at the stem top. Alternatively, channel block may include ion binding to Asp¹²⁷ and Asp¹²⁸, resulting in collapse of the barrel at the glycine-rich stem base. A mechanism to describe the rapid increase in pore conductance at low pH and the pH-dependent current fluctuations in the open channel (6), may involve protonation of one or more Glu¹¹¹ residues, disruption of Glu¹¹¹-Lys¹⁴⁷ ion pairs, and enlargement of the pore neck by rearrangement of Glu¹¹¹ and Lys¹⁴⁷ side chains. Although not poised in a constriction of the pore, Asp¹²⁷ and Asp¹²⁸ may participate in pH-dependent changes in conductance in α HL assembled on a cell membrane.

Rectification and reduction in pore conductance at high transmembrane potentials ($> \pm 100$ mV) may be understood in terms of varying degrees of conformational rearrangement and channel closure at the glycine-rich stem base. This region of the structure displays high thermal parameters and could undergo conformational changes leading to partial or complete steric block of the pore in response to an applied membrane potential. In fact, substitution of five histidine residues for Gly¹³⁰-Gly¹³⁴ yields a Zn²⁺-regulated pore that is closed by micromolar Zn²⁺ added from either the *cis* or *trans* sides of a bilayer apparatus (17). These experiments emphasize that the polypeptide backbone can undergo conformational rearrangements to yield a Zn²⁺ binding site

that reduces pore conductance, possibly via steric block of the pore. Alternatively, an applied membrane potential may alter the electrostatic potential in the pore, changing ion concentrations at the stem base and top, which in turn could affect permeant ion conduction and lead to the observed rectification behavior. Site-directed mutagenesis, structural studies, and biophysical experiments may now be used to test and refine specific molecular mechanisms.

The protomer structure and extensive biochemical information provide important insights into the structure of α_1 and mechanisms of assembly. Because the β sandwich forms a compact and well-ordered domain and there is little change in the secondary structure on heptamer formation (13), the water-soluble monomer probably has a tertiary fold that is similar to an α_7 protomer. Nonetheless, the amino latch and the glycine-rich stem exhibit greater exposure to aqueous solution in the α_1 state (13, 52). To prevent spontaneous assembly of α_1 to α_7 in aqueous solution and to maintain water solubility of α_1 , the hydrophobic residues of the stem β strands may pack against the nonpolar patch defined by Phe¹⁵³, Val¹⁶⁹, and Leu²¹⁹ (Fig. 5) in the α_1 state. By covering this hydrophobic cluster, assembly will be blocked until interaction with a membrane bilayer triggers strand rearrangement. In the α_1 , α_1^* , and α_7^* forms, the amino latch may participate in intraprotomer interactions with the inner surface of the β sandwich, some of which may be analogous to the interprotomer amino latch interactions in α_7 . Assembly of α HL is probably controlled by a tradeoff of intraprotomer interactions in the α_1 form for interprotomer and α_7 -membrane interactions in the α_7 form and thus may represent a prototype for bilayer-catalyzed folding and refolding.

α HL as a pore-forming motif for bacterial toxins. In contrast to a wide range of bacterial and insect toxins that utilize α -helices to perturb or penetrate the bilayer (55), the α HL heptamer structure defines the criteria for membership in a family of toxins that employ bilayer-spanning antiparallel β -barrels. The α HL protomer has secondary and tertiary structural features in common with aerolysin from *A. hydrophila*, whose structure is only known in the water-soluble form (56). Both protomeric species have long β strands that form a β sheet with a 180° twist, both have a domain containing numerous solvent-exposed tryptophan residues, and both toxins assemble to heptameric oligomers. The structure of the pore-forming domain of the α HL heptamer may define a more accurate model for the structure of the aerolysin pore-forming domain than the one obtained from fitting

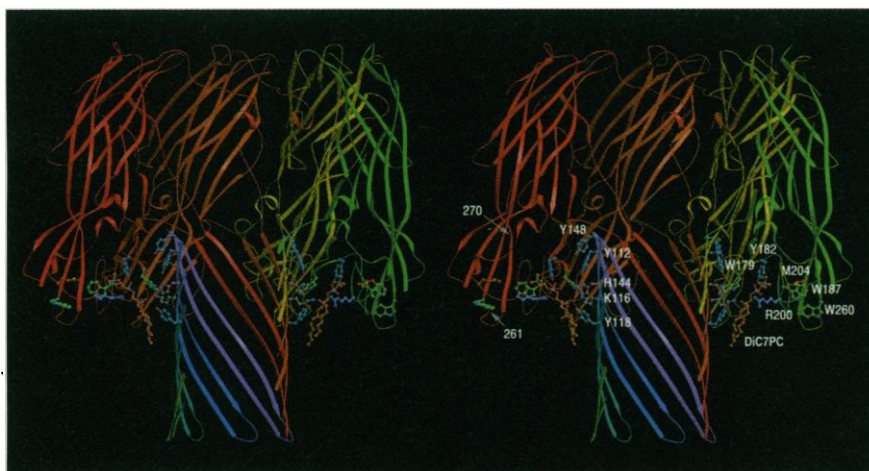


Fig. 6. A stereo view of a model for the interaction of the heptamer with phospholipid head groups. Difference electron density from α_7 crystals soaked in a solution containing DiC₇PC shows 5σ peaks near the guanidinium group of Arg²⁰⁰. We used the difference density in conjunction with chemical and biochemical information to guide the construction of a model for the interactions between α_7 and seven DiC₇PC molecules. Residues Tyr¹¹², Lys¹¹⁶, Tyr¹¹⁸, His¹⁴⁴, and Tyr¹⁴⁸ project from the surface of the stem, and Trp¹⁷⁹, Tyr¹⁸², Trp¹⁸⁷, Arg²⁰⁰, and Met²⁰⁴ define the rim side of the crevice, together forming an attractive binding site for phospholipid molecules.

the x-ray structure of the water-soluble form of aerolysin to low resolution electron density contours of the oligomer derived from image reconstruction of electron micrographs (56). Additional members of this family of β barrel, pore-forming toxins could include *Pseudomonas*-activated cytoxin and α toxin from *C. septicum*.

In conclusion, we have defined the structure of a bacterial toxin that assembles on the surface of eukaryotic cells and creates an aqueous transmembrane pore. The structure reveals the molecular basis for the biological activity of α HL from *S. aureus* and may provide insights into the structure of functionally related toxins such as aerolysin from *A. hydrophila*. The information reaped from our analysis of the α HL structure will facilitate protein engineering of the α HL channel (58) and may contribute to further understanding of the function and assembly of oligomeric membrane channels in general.

REFERENCES AND NOTES

1. S. Bhakdi, and J. Tranum-Jensen, *Microbiol. Rev.* **55**, 733 (1991).
2. J. E. Gouaux *et al.*, *Proc. Natl. Acad. Sci. U.S.A.* **91**, 12828 (1994).
3. A. Hildebrand, M. Pohl, S. Bhakdi, *J. Biol. Chem.* **266**, 17195 (1991).
4. G. Menestrina, *J. Membr. Biol.* **90**, 177 (1986).
5. Y. E. Korchev *et al.*, *ibid.* **143**, 143 (1995).
6. J. J. Kasianowicz and S. M. Bezrukov, *Biophys. J.* **69**, 94 (1995).
7. T. Tomita, M. Watanabe, T. Yasuda, *J. Biol. Chem.* **267**, 13391 (1992).
8. M. Watanabe, T. Tomita, T. Yasuda, *Biochim. Biophys. Acta* **898**, 257 (1987).
9. S. Bhakdi, R. Füssle, J. Tranum-Jensen, *Proc. Natl. Acad. Sci. U.S.A.* **78**, 5475 (1981).
10. N. T. Southall, J. J. Johnson, J. E. Gouaux, in preparation.
11. G. S. Gray and M. Kehoe, *Infect. Immun.* **46**, 615 (1984).
12. R. Füssle *et al.*, *J. Cell Biol.* **91**, 83 (1981).
13. N. Tobkes, B. A. Wallace, H. Bayley, *Biochemistry* **24**, 1915 (1985).
14. B. Walker, M. Krishnaswamy, L. Zorn, H. Bayley, *J. Biol. Chem.* **267**, 21782 (1992).
15. B. Walker, O. Braha, S. Cheley, H. Bayley, *Chem. Biol.* **2**, 99 (1995).
16. R. J. Ward, M. Palmer, K. Leonard, S. Bhakdi, *Biochemistry* **33**, 7477 (1994).
17. B. Walker, J. Kasianowicz, M. Krishnaswamy, H. Bayley, *Protein Eng.* **7**, 655 (1994).
18. B. E. Menzies and D. S. Kernodle, *Infect. Immun.* **62**, 1843 (1994).
19. M. Krishnaswamy, B. Walker, O. Braha, H. Bayley, *FEBS Lett.* **356**, 66 (1994).
20. B. Walker and H. Bayley, *J. Biol. Chem.* **270**, 23065 (1995).
21. B. Walker and H. Bayley, *Protein Eng.* **8**, 491 (1995).
22. R. Jursch *et al.*, *Infect. Immun.* **62**, 2249 (1994).
23. A. Valeva, M. Palmer, K. Hilgert, M. Kehoe, S. Bhakdi, *Biochim. Biophys. Acta* **1236**, 213 (1995).
24. J. E. Alouf and J. H. Freer, Eds., *Sourcebook of Bacterial Protein Toxins* (Academic Press, San Diego, CA, 1991).
25. M. C. Peitsch and J. Tschopp, *Curr. Opin. Cell Biol.* **3**, 710 (1991).
26. Monomeric α HL was isolated from cell culture supernatants of *Staphylococcus aureus* (Wood strain 46; ATCC 10832). Assembly was catalyzed by deoxycholate (9); and the heptamer was purified to homogeneity (as judged from SDS-PAGE, gel filtration, and analytical velocity and equilibrium ultracentrifugation data) by size exclusion chromatography in the presence of 40 mM *n*-octyl- β -glucoside.
27. L. Song and J. E. Gouaux, *Methods Enzymol.* **276**, 60 (1996); M. R. Hobaugh, L. Song, J. E. Gouaux, unpublished observation.
28. Parallelepiped of typical dimensions 0.4 by 0.3 by 0.2 nm³ were obtained after 2 to 4 weeks. Diffraction data were collected with the use of CuK α x-rays at room temperature and either an Enraf-Nonius FAST or a Rigaku R-Axis IIc area detector system. Integrated intensities were obtained from the FAST data by means of MADNES and PROCOR (29) and ROTAVATA/AGROVATA (30), and from the R-Axis data with the Rigaku PROCESS software. All data sets listed above were collected on the FAST system, except for the native data set II which was collected on the R-Axis. For the native data set II, three crystals were used. The strongest data from the three crystals were merged and reprocessed to generate the final ~14-fold redundant native data set.
29. A. Messerschmidt and J. W. Pflugrath, *J. Appl. Crystallogr.* **20**, 306 (1987).
30. "The CCP4 suite: Programs for protein crystallography," *Acta Crystallogr.* **D50**, 760 (1994).
31. Crystals were transferred to mother liquor solutions containing either 5 mM UO₂Cl₂, 10 mM OsCl₃, 50 mM K₂O₈, or 50 mM K₃IrCl₆ and soaked for 1 to 2 weeks. The major uranyl and osmium sites were determined by inspection of difference Patterson maps. Difference Fourier maps were used to locate minor sites and sites in other derivatives. Heavy atom positions were refined with XHeavy in the XtalView package (32) and phases were calculated with the program PHASES (33). A MIR electron density map was calculated at 3.0 Å resolution from which a protein-solvent boundary could be discerned as well as prominent elements of secondary structure. Density modification which included solvent flattening, histogram matching, and noncrystallographic symmetry averaging by means of the program DM (37) improved the quality of the electron density map. DM was also used for phase extension from 3.0 to 2.4 Å and from 3.0 Å to 1.9 Å with the FAST and R-Axis IIc data sets, respectively.
32. D. E. McRee, *J. Mol. Graph.* **10**, 44-46 (1992).
33. W. Furey and S. Swaminathan, *Methods Enzymol.*, in press.
34. B.-C. Wang, *Methods Enzymol.* **115**, 90 (1985).
35. K. Y. J. Zhang and P. Main, *Acta Crystallogr.* **A46**, 41 (1990).
36. M. G. Rossmann and D. M. Blow, *Acta Crystallogr.* **16**, 39 (1963); G. Bricogne, *ibid.* **A30**, 395 (1974).
37. K. Cowtan, *Joint CCP4 and ESF-EACBM Newsletter on Protein Crystallography* **31**, 34 (1994).
38. Initial structures for a protomer were independently built into the 2.4 Å map with Xfit (32) and Bones-Lego-O (39). Both models yielded the same trace and similar side chain positions. The six additional protomers were obtained by application of the noncrystallographic symmetry (NCS) transformations followed by manual readjustments, first in the 2.4 Å map and then in the 1.9 Å map.
39. T. A. Jones, J.-Y. Zou, S. W. Cowan, M. Kjeldgaard, *Acta Crystallogr.* **A47**, 110 (1991).
40. A. T. Brünger, *X-PLOR. Version 3.1. A System for X-ray Crystallography and NMR* (Yale Univ. Press, New Haven, 1992).
41. The structure was refined with X-PLOR (40), beginning from a crystallographic *R* value of 40.5 percent at 2.4 Å resolution. This was followed by alternating cycles of manual refitting to both $2|F_o| - |F_c|$ and $|F_o| - |F_c|$ omit maps and refinement of atomic positions and *B* factors. Before the solvent was added, the conventional *R* value was 0.229 and the free *R* value was 0.288 with good stereochemistry. Because the electron density features at the base of the stem and rim regions are weak, these regions were rebuilt into $|F_o| - |F_c|$ omit maps that were averaged around the noncrystallographic sevenfold axis. In the last three cycles of refinement, NCS restraints were placed on the main-chain (25 kcal mol⁻¹ Å⁻²) and side chain (4 kcal mol⁻¹ Å⁻²) atoms of residues 119 to 140 and on the main chain atoms (25 kcal mol⁻¹ Å⁻²) of residues 260 to 265. Because of poor side chain density, residues Arg⁶⁶ and Lys⁷⁵ (A protomer), Lys³⁰ (D), Lys²⁴⁰ (D), Lys²⁸³ (F) and Lys³⁰ (G) were replaced by alanine (A). Analysis of the structure by PROCHECK (57) indicates that all residues occupy allowed regions of the Ramachandran plot.
42. Figures were created from the following programs. MOLSCRIPT: P. J. Kraulis, *J. Appl. Crystallogr.* **24**, 946 (1991); RASTER3D: E. A. Merritt, M. E. P. Murphy, *Acta Crystallogr.* **D50**, 869 (1994); XtalView (32); GRASP: A. Nicholls, K. A. Sharp, B. Honig, *Proteins: Struct. Funct. Genet.* **11**, 281 (1991); SETOR: S. V. Evans, *J. Mol. Graphics*, **11**, 134 (1993).
43. R. J. Ward and K. Leonard, *J. Struct. Biol.* **109**, 129 (1992).
44. A. G. Murzin, S. E. Brenner, T. Hubbard, C. Chothia, *J. Mol. Biol.* **247**, 536 (1995).
45. H. Iikgai and T. Nakae, *Biochem. Biophys. Res. Commun.* **130**, 175 (1985).
46. R. A. Paupit *et al.*, *J. Struct. Biol.* **107**, 136 (1991).
47. T. Schirmer, T. A. Keller, Y.-F. Wang, J. P. Rosenbusch, *Science* **267**, 512 (1995).
48. A. D. McLachlan, *J. Mol. Biol.* **128**, 49 (1979); A. G. Murzin, A. M. Lesk, C. Chothia, *ibid.* **236**, 1369, 1382 (1994).
49. A. Karlin, M. H. Akabas, *Neuron* **15**, 1231 (1995).
50. R. W. Pastor, R. M. Venable, M. Karplus, *Proc. Natl. Acad. Sci. U.S.A.* **88**, 892 (1991); N. P. Franks, *J. Mol. Biol.* **100**, 345 (1976).
51. D. M. Surgenor, Ed., *The Red Blood Cell* (Academic Press, New York, 1974), vol. 1.
52. A. Valeva *et al.*, *EMBO J.* **15**, 1857 (1996).
53. C2 crystals grown in the presence of *n*-octyl- β -glucoside were soaked in 1 mM DiC₇-PC and a total of 441,355 observations of 119,211 independent reflections were measured at room temperature. The reduced data set was 72.4 percent complete to 2.1 Å resolution, with a merging *R* value on intensities of 9.8 percent. The model for DiC₇-PC was based on high-resolution phospholipid crystal structures [H. Hauser, I. Pascher, R. H. Pearson, S. Sundell, *Biochim. Biophys. Acta* **650** 21 (1981)].
54. O. V. Krasilnikov, R. Z. Sabirov, V. I. Ternovsky, P. G. Merzliak, B. A. Tashmukhamedov, *Gen. Physiol. Biophys.* **7**, 467 (1988).
55. J. Li, *Curr. Opin. Struct. Biol.* **2**, 545 (1992).
56. M. W. Parker *et al.*, *Nature* **367**, 292 (1994).
57. R. A. Laskowski, M. W. MacArthur, D. S. Moss, J. M. Thornton, *J. Appl. Crystallogr.* **26**, 283 (1993).
58. H. Bayley, *Bioorg. Chem.* **23**, 340 (1995).
59. We thank A. Balciunas for crystallization assistance; K. Cowtan, P. Loll, B. Perman, D. Picot, B. Ramachandran, Z. Ren, X.-J. Yang, and members of the Bayley, Gouaux, Garavito, and Moffat groups for assistance and comments; and H.-M. Ke (U. of North Carolina) for area detector time and helpful suggestions. Supported in part by funds from a PHS/NIH Shared Instrumentation Grant and a Lou- is Block grant, respectively, for the FAST and R-Axis IIc area detectors. Initial refinement was performed at the Pittsburgh Supercomputer Center. This work was supported in part by grants from the Office of Naval Research (J.E.G. and H.B.), the NIH (J.E.G.), the Martin D. and Virginia S. Kamen Sustaining Fund for Junior Faculty (J.E.G.), the Searle Scholars Program (J.E.G.), the NSF (J.E.G.), and the DOE (H.B.), the Cancer Research Foundation Young Investigator Fund (J.E.G.), and the Medical Scientist Training Program at the University of Chicago (M.R.H.). The coordinates have been deposited at the Protein Data Bank at Brookhaven with accession number 7ahl.

30 July 1996; accepted 21 October 1996